NANO LETTERS

2007
Vol. 7, No. 4
1037−1043

Direct Observation of sp−d Exchange Interactions in Colloidal Mn^{2+}- and Co^{2+}-Doped CdSe Quantum Dots

Paul I. Archer, Steven A. Santangelo, and Daniel R. Gamelin*

Department of Chemistry, University of Washington, Seattle, Washington 98195-1700

Received January 29, 2007; Revised Manuscript Received March 9, 2007

ABSTRACT

The defining attribute of a diluted magnetic semiconductor (DMS) is the existence of dopant−carrier magnetic exchange interactions. In this letter, we report the first direct observation of such exchange interactions in colloidal doped CdSe nanocrystals. Doped CdSe quantum dots were synthesized by thermal decomposition of $(Me_4N)_2[Cd_4(SePh)_{10}]$ in the presence of $TMCl_2$ ($TM^{2+} = Mn^{2+}$ or Co^{2+}) in hexadecylamine and were characterized by several analytical and spectroscopic techniques. Using magnetic circular dichroism spectroscopy, successful doping and the existence of giant excitonic Zeeman splittings in both Mn^{2+}- and Co^{2+}-doped wurtzite CdSe quantum dots are demonstrated unambiguously.

Diluted magnetic semiconductor (DMS)[1] nanostructures are the basic working components of many existing and proposed devices in the emerging field of semiconductor spin-based electronics, or spintronics.[2−4] Prototype spin valves and spin-based light-emitting diodes have been demonstrated that use DMS nanostructures grown by molecular beam epitaxy as their key functional components.[2−8] The novel functionalities of these devices all derive from carrier−dopant magnetic exchange interactions within the DMSs (the so-called sp−d exchange interactions).[1] These exchange interactions allow the manipulation of carrier spins through magnetization of the magnetic impurities.

A central theme of the field of nanotechnology is the use of bottom-up approaches for the preparation of device structures analogous to those grown by molecular beam epitaxy or related vacuum deposition techniques. Various functional devices, including field-effect transistors, light-emitting diodes, and sensors, have been made by self-assembly of colloidal nanocrystalline components.[9,10] Recently, focus has shifted toward doping of colloidal semiconductor nanocrystals by direct chemical methods because of the vast untapped potential to control their physical properties through the judicious introduction of impurities.[11,12] CdSe is arguably the most thoroughly investigated of the binary semiconductors made by colloidal chemistry methods, but doping of this lattice has been notoriously problematic.[13−15] Several groups have claimed successful doping of CdSe nanocrystals by direct chemical methods,[13,14,16−22] mostly with magnetic transition metal (TM^{2+}) impurity ions such as Mn^{2+}. The evidence supporting these claims has included: (i) insensitivity of some observable (e.g., magnetic susceptibility, electron paramagnetic resonance (EPR) spectrum) to pyridine surface ligand exchange, (ii) Vegard's law behavior in the X-ray diffraction (XRD), and (iii) observation of resolved six-line hyperfine structure in Mn^{2+} EPR spectra. Unfortunately, the very small dopant concentrations and very large surface-to-volume ratios of the nanoparticles often described in the literature (e.g., 1−10 dopants/4 nm diameter nanocrystal) make false positives a major concern.[23] For each of the above criteria, for example, counterexamples have been encountered: (i) pyridine can be exceedingly slow in removing TM^{2+} ions with two or more bonds to a nanocrystal surface,[24] (ii) core/shell nanostructures can show shifts in XRD lines similar to those expected from Vegard's law for alloys,[11,25,26] and (iii) Mn^{2+} in various chalcogenide impurity phases can show EPR hyperfine splittings similar to those expected for Mn^{2+} in doped II−VI chalcogenide nanocrystals. Because of the numerous scenarios that may lead to false positives, claims of nanocrystal doping must be substantiated by extraordinarily strong evidence in favor of that conclusion.

The defining feature of a true DMS is the existence of sp−d exchange coupling between the dopants and semiconductor band electrons.[1] To date, physical properties deriving from sp−d exchange have not been demonstrated for any colloidal doped CdSe nanocrystals. An experiment sensitive to the existence of sp−d exchange coupling in colloidal TM^{2+}:CdSe nanocrystals would therefore provide a powerful avenue for testing claims of successful doping and, in contrast with the various methods listed above, would also allow the

* To whom correspondence should be addressed. E-mail: gamelin@chem.washington.edu.

10.1021/nl0702362 CCC: $37.00
Published on Web 03/23/2007

functionally relevant physical properties of the doped nanocrystals to be evaluated.

In this letter, we report the first direct observation of sp−d exchange interactions in colloidal TM^{2+}-doped CdSe quantum dots (QDs). Magnetic circular dichroism (MCD) spectroscopy is used as a direct probe of sp−d exchange interactions in DMS nanocrystals, revealing giant excitonic Zeeman splittings through differential absorption of left (σ^-) and right (σ^+) circularly polarized light. MCD spectra of colloidal DMS QDs demonstrate successful doping of both Mn^{2+} and Co^{2+} into 2−5 nm diameter wurtzite CdSe nanocrystals and confirm the existence of giant excitonic Zeeman splittings in these doped QDs. The results presented here show that these TM^{2+}-doped CdSe nanocrystals are promising materials for studying spin effects in semiconductor nanostructures.

Doped CdSe nanocrystals were prepared by a variation of the cluster method advocated by the Strouse group.[16] Briefly, the cluster precursor $(Me_4N)_2[Cd_4(SePh)_{10}]$ was synthesized by adapting literature methods[27] to use benzeneselenol in place of benzenethiol. The selenol-terminated inorganic cluster was prepared under inert (N_2) conditions by addition of $Cd(NO_3)_2{\cdot}4H_2O$ (17 mmol) in methanol (15 mL) to an equimolar solution of triethylamine and benzeneselenol (45 mmol) in methanol (15 mL) at room temperature. A solution of tetramethylammonium chloride (19 mmol) in methanol (10 mL) was added, and the mixture was allowed to crystallize at 0 °C under N_2. The crystalline product was filtered, washed repeatedly with methanol, and dried under vacuum.

To our knowledge, neither $(Me_4N)_2[Cd_4(SePh)_{10}]$ nor related selenol-capped clusters have been used previously to prepare doped CdSe nanocrystals, although a related cluster has been reported to yield undoped CdSe nanocrystals when heated under conditions similar to ours.[28] In our experience, however, the use of benzeneselenol in place of benzenethiol appears to be essential for achieving the correct TM^{2+}:CdSe product. As will be described in detail elsewhere,[29] attempts to synthesize Co^{2+}- and Mn^{2+}-doped CdSe using a similar thiol-terminated cluster $(Me_4N)_4[Cd_{10}Se_4(SPh)_{16}]$ resulted in crystal lattice segregation.

TM^{2+}:CdSe QDs were synthesized from the $(Me_4N)_2[Cd_4(SePh)_{10}]$ clusters by techniques adapted from literature involving $(Me_4N)_4[Cd_{10}Se_4(SPh)_{16}]$.[30] To synthesize TM^{2+}:CdSe QDs, a solution of 0−0.3 mmol of $TMCl_2$ in 11.8 g of hexadecylamine was degassed under vacuum at 130 °C for 1.5 h. The reaction vessel was placed under N_2 and the temperature reduced to <80 °C, at which point 0.1 mmol of $(Me_4N)_2[Cd_4(SePh)_{10}]$ and 0.27 mmol of Se powder were introduced. The temperature was increased to 130 °C and maintained for 1.5 h. The temperature was then slowly increased to 215 °C and kept constant until the desired QD size was achieved. After growth, the solution was rapidly cooled to <100 °C, and the particles were isolated by addition of a mixture of toluene and methanol, followed by centrifugation and resuspension in toluene. The process of precipitation with methanol followed by resuspension in toluene was repeated three times to remove excess reagents. Surface-bound dopants were removed by sonicating the suspended QDs in the presence of trioctyl-phosphine oxide (TOPO), followed by precipitation, centrifugation, and resuspension in toluene. Surface cleaning of Co^{2+}:CdSe nanocrystals was monitored by UV/vis absorption spectroscopy as described in previous reports.[24,31−33]

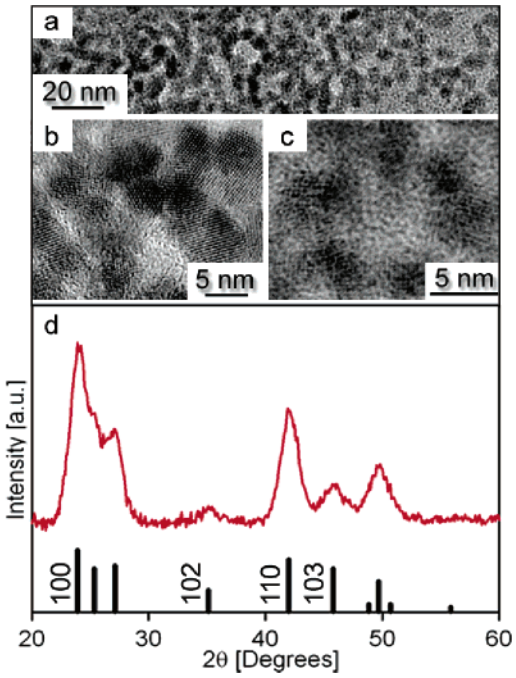

Figure 1. TEM images of (a,b) 2.1% Co^{2+}:CdSe and (c) 1.0% Mn^{2+}:CdSe nanocrystals. (d) X-ray diffraction data of $d = 4.6$ nm ~0.1% Mn^{2+}:CdSe nanocrystals. The vertical bars show the diffraction peak positions of bulk wurtzite CdSe.

Figure 1 presents representative TEM images of (a,b) 2.1% Co^{2+}:CdSe, (c) 1.0% Mn^{2+}:CdSe, and (d) powder XRD data for ~0.1% Mn^{2+}:CdSe QDs. The nanocrystals appear approximately spherical and exhibit XRD peak positions matching those of wurtzite CdSe. A Scherrer[34] analysis of the 110 peak yields an average diameter of ca. 4.6 nm, consistent with the diameter (4.58 nm) estimated from established relationships[35] between CdSe band gap energies and nanocrystal diameters. In general, nanocrystals ranging from 2.5−5.0 nm in diameter and with 0−2% TM^{2+} incorporation can be prepared by this method through appropriate control of the synthetic conditions.

Electronic absorption spectroscopy provides evidence for successful Co^{2+} incorporation into the CdSe QDs. Figure 2 presents 300 K electronic absorption spectra of colloidal 1.5% Co^{2+}:CdSe QDs suspended in toluene. Both the $^4A_2(F) \rightarrow {}^4T_1(P)$ ligand-field transition (~13 500 cm^{-1}, or 1.67 eV) of tetrahedral cobalt and the well-defined excitonic transition (~18 700 cm^{-1}, or 2.32 eV) of the $d = 2.76$ nm CdSe nanocrystals are observed. This Co^{2+} absorption band agrees well with that of bulk Co^{2+}:CdSe,[36] with the exception that the $^4T_1(P)$ band in bulk Co^{2+}:CdSe is partially occluded by the onset of the CdSe band edge, whereas in the Co^{2+}:CdSe QDs, the $^4T_1(P)$ band is clearly resolved because the CdSe band edge absorption has shifted to higher energy due

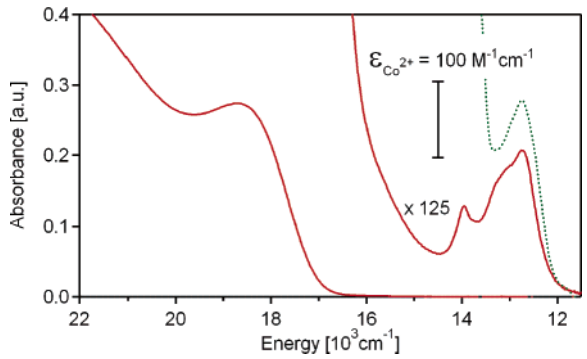

Figure 2. Absorption spectra at 300 K of colloidal $d = 2.76$ nm 1.5% Co^{2+}:CdSe QDs suspended in toluene. The dashed line shows the absorption spectrum of bulk Co^{2+}:CdSe in the $^4A_2(F) \rightarrow {}^4T_1(P)$ ligand-field region (adapted from ref 36).

to quantum confinement. The molar absorptivity ($\epsilon_{Co^{2+}} \approx 200\ M^{-1}\ cm^{-1}$) is consistent with four-coordinate Co^{2+} in other II−VI nanocrystals.[24,33,37] Previously, ligand-field electronic absorption spectroscopy was used to monitor changes in Co^{2+} speciation during nanocrystal doping, allowing distinction between surface and substitutional Co^{2+} in Co^{2+}:ZnO[31,33] and Co^{2+}:CdS,[24] for example. As in these cases, Co^{2+} ions bound to the surfaces of CdSe nanocrystals show broadened absorption bands shifted to higher energies than those of substitutional Co^{2+} in CdSe (see Supporting Information), reflecting inhomogeneous speciation and the greater effective ligand-field strengths of the surface-capping ligands than the lattice Se^{2-} anions. After surface cleaning, there is no evidence from the ligand-field spectroscopy of any remaining surface bound Co^{2+} in these Co^{2+}:CdSe nanocrystals.[29]

Mn^{2+}:CdSe QDs were prepared in the same manner. Because Mn^{2+} has no spin-allowed ligand-field transitions, only the transitions of CdSe were observed in the absorption spectrum. EPR spectroscopy was therefore chosen as a more suitable technique for characterizing Mn^{2+} speciation. Figure 3 plots the 300 K X-band EPR spectrum of colloidal ∼0.1% Mn^{2+}:CdSe QDs ($d = 4.58$ nm) suspended in toluene. The experimental spectrum shows the characteristic six-line hyperfine splitting pattern of Mn^{2+} (^{55}Mn, I = 5/2) with sufficient resolution to identify several smaller features between the six principal lines.

$$\hat{H} = g\mu_B \mathbf{H}\cdot\mathbf{S} + A\mathbf{S}\cdot\mathbf{I} + D\left[S_z^2 - \frac{1}{3}S(S+1)\right] \qquad (1)$$

The experimental EPR spectrum was simulated by using the axial spin Hamiltonian of eq 1, which includes the Zeeman splitting, electron−nuclear hyperfine coupling, and axial zero-field splitting terms, respectively. The g factor and hyperfine (A) values were approximated as isotropic because their spectral anisotropy would be poorly resolved in the powder EPR spectrum of Mn^{2+}:CdSe. The fine structure could not be reproduced without inclusion of an axial zero-field splitting, consistent with Mn^{2+} substitution for Cd^{2+} at the axially distorted cation site of wurtzite CdSe. D-strain on the order of 7% was included to account for inhomogeneous broadening. The resulting simulation is shown in Figure 3. The g and A parameters deduced from the simulation ($g_{iso} = 2.0041 \pm 0.0005$, $A_{iso} = (-62.2 \pm 0.1) \times 10^{-4}\ cm^{-1}$) agree well with those reported for bulk Mn^{2+}:CdSe ($g_{iso} = 2.0041 \pm 0.0005$, $A_{iso} = (-62.2 \pm 0.1) \times 10^{-4}\ cm^{-1}$).[38] This prior analysis of the bulk Mn^{2+}:CdSe EPR spectrum used a spin Hamiltonion that included additional cubic field and fourth-order spin−orbit perturbations not included in eq 1. As a result, the two simulations yield different values for the second-order spin−orbit coupling parameter D: $D = -82 \times 10^{-4}\ cm^{-1}$ from eq 1, compared to $D = (+15.2 \pm 0.5) \times 10^{-4}\ cm^{-1}$ in ref 38. The powder EPR spectrum of Figure 3 is reproduced well using the simpler Hamiltonian of eq 1, but the resulting D value must be viewed as an effective phenomenological number and should not be overinterpreted. Because inclusion of additional higher-order terms would result in overparameterization, it is not warranted by the data. Both g_{iso} and A_{iso} are unaffected by this approximation. We note that the hyperfine coupling constant, A_{iso}, obtained in Figure 3 is significantly smaller than that determined previously for Mn^{2+} in colloidal wurtzite Mn^{2+}:ZnO nanocrystals using the same spin Hamiltonian ($g_{iso} = 1.999$, $A_{iso} = -74.0 \times 10^{-4}\ cm^{-1}$, $D = -2.36 \times 10^{-2}$),[39] suggesting greater delocalization of unpaired spin density away from the Mn^{2+} nuclei (i.e., greater Mn^{2+}-anion covalency) in the Mn^{2+}:CdSe QDs. Overall, the EPR analysis corroborates the conclusion reached for Co^{2+}:CdSe nanocrystals above, namely that this synthetic method results in successful TM^{2+} doping of wurtzite CdSe nanocrystals.

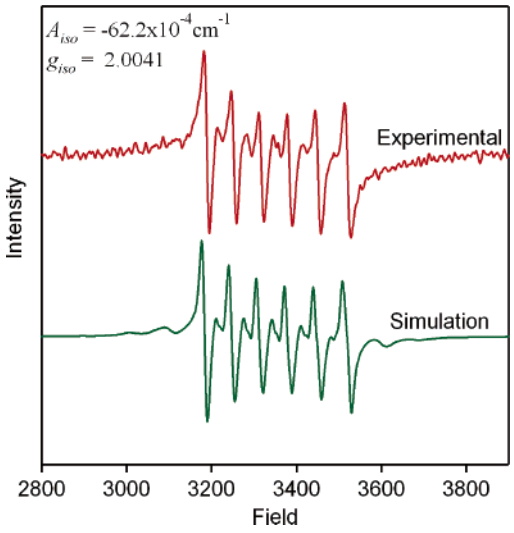

Figure 3. Experimental (top) and simulated (bottom) 300 K X-band EPR spectra of colloidal $d = 4.58$ nm ∼0.1% Mn^{2+}:CdSe nanocrystals suspended in toluene. The sample is the same as used for Figure 1d. The simulation was performed using eq 1 ($g_{iso} = 2.0041 \pm 0.0005$, $A_{iso} = -62.2 \pm 0.1 \times 10^{-4}\ cm^{-1}$, $D = -82 \times 10^{-4}\ cm^{-1}$, 7% D-strain).

As described above, the data in Figures 1−3 provide strong evidence for nanocrystal doping but do not provide a direct demonstration of sp−d exchange interactions in these quantum dots. To probe for sp−d exchange coupling, MCD spectroscopy was used to measure the excitonic Zeeman splittings of the nanocrystals with and without TM^{2+} dopants.

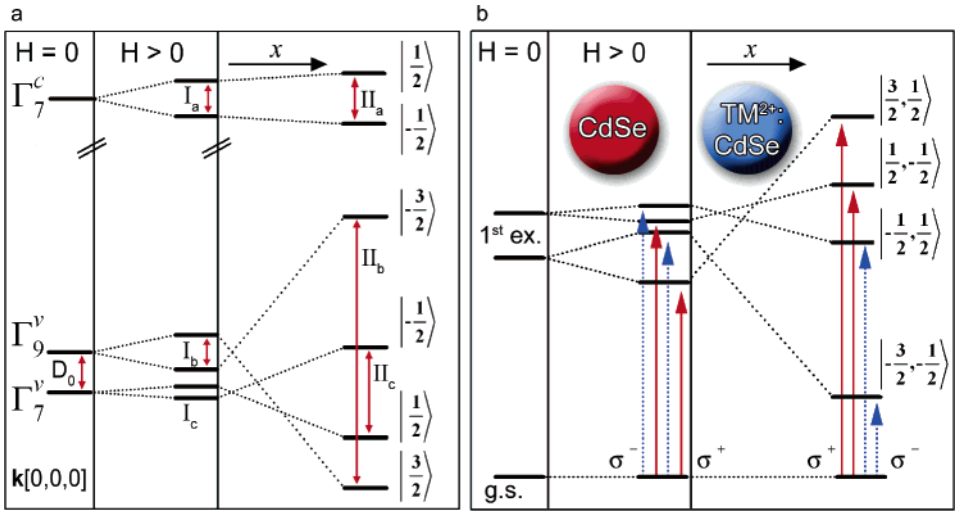

Figure 4. (a) Zeeman splittings of wurtzite CdSe valence (Γ_7^v and Γ_9^v) and conduction (Γ_7^c) one-electron levels in the presence of a magnetic field ($H > 0$) and their dependence on transition metal dopant concentration (x) in TM^{2+}:CdSe. The splitting energies are given by I_a, I_b, I_c, and II_a, II_b, II_c. See text for details. (b) Multielectron state diagram illustrating the band-edge transitions probed by MCD spectroscopy, where σ^- and σ^+ correspond to the absorption of left and right circularly polarized light, respectively.

Adopting the formalism used to describe the analogous bulk DMSs,[1] the Zeeman splittings of the one-electron semiconductor valence (Γ_7^v and Γ_9^v) and conduction (Γ_7^c) levels at the Γ point for both undoped and doped CdSe are summarized in Figure 4a. The corresponding multielectron state diagrams that describe the observed MCD spectroscopy at the band edge are shown in Figure 4b.

At zero field ($H = 0$), the valence band of hexagonal CdSe is split into Γ_7^v and Γ_9^v levels separated by the crystal-field splitting energy $D_0 \approx 195$ cm^{-1} (~24 meV).[1] Application of a magnetic field ($H > 0$) splits the valence and conduction (Γ_7^c) one-electron levels according to their intrinsic g_e and g_{hh} values (Figure 4b). Within this Zeeman-split manifold, there are four optical transitions allowed by the selection rules for absorption of circularly polarized light ($\Delta m_J = \pm 1$) and four that are forbidden in circular polarization. The Zeeman splitting energies of the valence and conduction levels shown in Figure 4a are: $I_a = g_e\mu_B H$, $I_b = 3g_{hh}\mu_B H$, and $I_c = g_{hh}\mu_B H$. The effective excitonic Zeeman splitting energy for an undoped CdSe QD, defined here as the energy difference $\Delta E_{Zeeman} = |-3/2,-1/2\rangle - |3/2,1/2\rangle$ in Figure 4b (where the notation describes the parent $|h_{vb}^+,e_{cb}^-\rangle$ configuration), is thus given by eq 2, and the effective Landé g factor is defined as $g_{eff} = \Delta E_{Zeeman}/\mu_B H$. Because the g values of wurtzite CdSe are anisotropic, those measured for a frozen solution of CdSe nanocrystals are orientation-averaged. The excitonic MCD signal is derivative shaped due to the overlap of equal and opposite bands separated in energy by ΔE_{Zeeman} (i.e., an A-term MCD signal[40]). From eq 2, ΔE_{Zeeman} of diamagnetic CdSe is expected to be linearly proportional to the applied magnetic field strength. Following the sign convention of Piepho and Schatz,[40] a positive g_{eff} of the first transition would yield a positive A-term signal, whereas a negative g_{eff} would yield a negative A-term signal.

$$\Delta E_{Zeeman} = (3g_{hh} - g_e)\mu_B H \qquad (2)$$

Exchange coupling between the exciton and magnetic dopants introduces a new contribution to the excitonic Zeeman splitting energy. This contribution depends on the strengths of the TM^{2+}-carrier exchange interactions $N_0\alpha$ (s−d, or potential exchange) and $N_0\beta$ (p−d, or kinetic exchange), and on the effective concentration of TM^{2+} ions (x). In the limit of zero applied field, the random spin orientations of an ensemble of TM^{2+} ions lead to net cancellation of the exchange term and consequently $\Delta E_{Zeeman} = 0$. In the limit of one TM^{2+} ion, the exchange splitting occurs even in the absence of an applied magnetic field but is averaged out in an ensemble measurement.[41−43] As the TM^{2+} spins are aligned by an external magnetic field, their exchange energies add constructively, and a dopant-dependent contribution to ΔE_{Zeeman} is observed. ΔE_{Zeeman} is therefore dependent upon the spin expectation value for the TM^{2+} dopants along the direction of the applied magnetic field, $\langle S_z\rangle$ (note that $\langle S_z\rangle$ is defined as a negative quantity[1]). The Zeeman splitting energies of the valence and conduction levels shown in Figure 4a for the doped CdSe QDs are then: $II_a = I_a - x\langle S_z\rangle N_0\alpha$, $II_b = x\langle S_z\rangle N_0\beta - I_b$, and $II_c = (1/3)x\langle S_z\rangle N_0\beta - I_c$, and the effective excitonic Zeeman splitting energy in the TM^{2+}:CdSe DMS QDs is described by eq 3. In both Mn^{2+}:CdSe and Co^{2+}:CdSe bulk DMSs, $N_0\alpha > 0$ and $N_0\beta \ll 0$.[1] The sp−d term in eq 3 thus opposes the intrinsic Zeeman splitting of the exciton and, if large enough, should cause an inversion of the MCD A-term polarity at the band edge (Figure 4b).

$$\Delta E_{Zeeman} = (3g_{hh} - g_e)\mu_B H + x\langle S_z\rangle N_0(\alpha - \beta) \qquad (3)$$

Figure 5 shows 6 K absorption and variable-field (0−5 T) MCD spectra of TOPO-capped (a) $d = 3.19$ nm CdSe, (b) $d = 2.64$ nm 1.0% Mn^{2+}:CdSe, and (c) $d = 2.76$ nm 1.5% Co^{2+}:CdSe nanocrystals. The MCD features of the undoped CdSe QDs (Figure 5a) centered at ca. 20 000 cm^{-1} (2.48 eV) are similar to those reported previously.[44,45] As

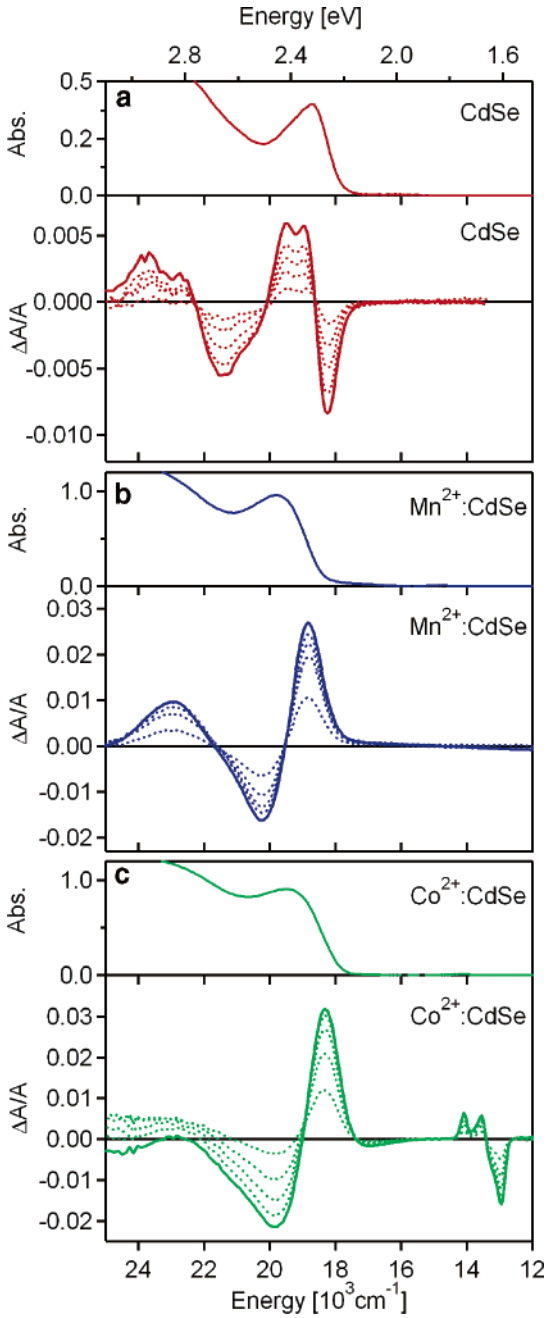

Figure 5. Electronic absorption and variable field (0−5 T) MCD spectra of colloidal (a) $d = 3.19$ nm, undoped CdSe nanocrystals, (b) $d = 2.64$ nm, 1.0% Mn^{2+}:CdSe nanocrystals, and (c) $d = 2.76$ nm, 1.5% Co^{2+}:CdSe nanocrystals collected at 6 K.

described previously,[45] the first two excited states in undoped CdSe have g_{eff} values with opposite signs, giving rise to two overlapping *A*-term MCD signals with opposite polarities. The leading *A*-term derivative in Figure 5a is positive, indicating $g_{eff} > 0$ for this excited state. Variable-field measurements of the CdSe QDs show no saturation but only a linear dependence of the MCD intensity on field (Figure 6).

The 1.0% Mn^{2+}:CdSe QDs also show a derivative-shaped MCD feature at ca. 19 500 cm^{-1} (Figure 5b), but with significantly more intensity (ca. 30 times) and an inverted polarity relative to the undoped CdSe QDs. Similarly, the

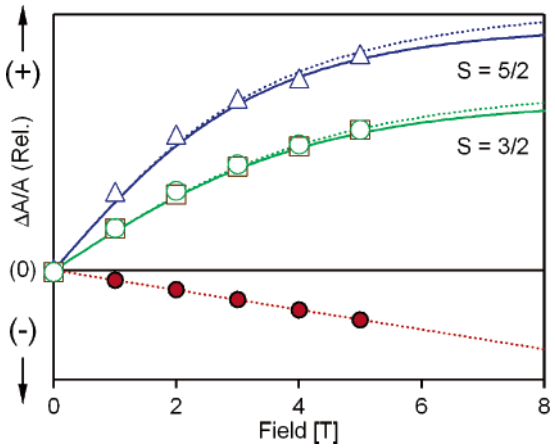

Figure 6. Variable-field MCD saturation magnetization data collected at 6 K for the samples from Figure 5. Undoped CdSe (●, exciton), 1.0% Mn^{2+}:CdSe (△, exciton), 1.5% Co^{2+}:CdSe (□, exciton; ○, $^4T_1$(P) ligand-field). The dashed curves show the spin-only saturation magnetization calculated from eq 4 using appropriate bulk parameters (Mn^{2+}: $g = 2.0041$, $S = 5/2$; Co^{2+}: $g = 2.3$, $S = 3/2$).[38,46] The solid curves show the results expected from inclusion of the first term in eq 3. The dashed straight line is a linear fit of the CdSe data.

excitonic MCD feature of the 1.5% Co^{2+}:CdSe QDs is more intense and inverted in polarity relative to undoped CdSe. In addition to excitonic intensity, the MCD spectra of the Co^{2+}:CdSe QDs show a second feature at ~13 500 cm^{-1} that is readily identified as the spin−orbit split $^4A_2$(F) → $^4T_1$(P) ligand-field transition of tetrahedral Co^{2+} (see Figure 2).

A salient feature of the TM^{2+}-doped CdSe QD MCD intensities is their saturation magnetization in variable-field measurements (Figure 6). In contrast to the intensities of the undoped CdSe QDs, the excitonic MCD intensities of Mn^{2+}- and Co^{2+}-doped CdSe QDs saturate, following the ground-state saturation magnetization of these ions ($S = 5/2$ and $S = 3/2$, respectively). The dashed curves in Figure 6 show the relative magnetizations of $S = 5/2$ and $S = 3/2$ ions calculated from eq 4 using the isotropic g values measured for bulk Mn^{2+}- and Co^{2+}-doped CdSe (2.0041 (Figure 3) and $g = 2.3$,[46] respectively), where M is the volume magnetization, N_0 is the number of unit cells per unit volume, x is the cation mole fraction of paramagnetic ions, μ_B is the Bohr magneton, T is the temperature, H is magnetic field, and k is Boltzmann's constant. The zero-field splittings of the Mn^{2+} and Co^{2+} ground states have been neglected because, in both cases, $2D$ is sufficiently smaller than kT at 6 K ($D = 0.0082$ cm^{-1} for Mn^{2+}:CdSe (Figure 3) and 0.5 cm^{-1} for Co^{2+}:CdSe[46]).

$$M = -N_0 x g \mu_B \langle S_z \rangle$$
$$= \frac{1}{2} N_0 x g \mu_B \left[(2S+1) \coth\left((2S+1)\left(\frac{g\mu_B H}{2kT}\right)\right) - \coth\left(\frac{g\mu_B H}{2kT}\right)\right] \quad (4)$$

For Mn^{2+}:CdSe, the excitonic MCD saturation magnetization data in Figure 5 follow the anticipated $S = 5/2$

Table 1. Comparison of Excitonic Zeeman Splitting Energies in Undoped and TM^{2+}-Doped CdSe Quantum Dots

sample	TM^{2+}/QD (av)	ΔE_{Zeeman} (6 K, 5 T) (meV)	ΔE_{Zeeman}(saturation) exptl (meV)	predicted[a] (meV)	exptl vs predicted (%)	g_{eff} (6 K)
1.0% Mn^{2+}:CdSe ($d = 2.64$ nm)	1.7	−9.4	−11.5	−24.3	47	−52.5
1.5% Co^{2+}:CdSe ($d = 2.76$ nm)	2.9	−10.2	−13.3	−30.4	44	−49.7
CdSe ($d = 3.19$ nm)	0	+0.31	--	--	--	+1.1

[a] Calculated from bulk $N_0(\alpha-\beta)$ values[1,49] using eqs 3 and 4 and $T = 6$ K.

magnetization very well. Similarly, for Co^{2+}:CdSe, the excitonic and ligand-field MCD intensities both follow the same $S = 3/2$ magnetization. The observation of TM^{2+} saturation magnetization for the excitonic MCD intensities unequivocally demonstrates exciton−TM^{2+} exchange coupling in both Mn^{2+}:CdSe and Co^{2+}:CdSe QDs. The inverted polarities of the first MCD signal relative to undoped CdSe further indicate that the sp−d exchange contribution dominates eq 3 for both Mn^{2+}:CdSe and Co^{2+}:CdSe QDs. In fact, description of the data in Figure 5 using eq 4 is only approximate because it neglects the first term in eq 3, but this intrinsic term is small relative to the sp−d term (vide infra) and is therefore usually neglected. Explicit inclusion of the intrinsic splitting term yields the solid curves in Figure 5.

When ΔE_{Zeeman} is small relative to the CdSe crystal-field splitting, D_0, the experimental excitonic Zeeman splitting energy can be estimated from the absorption and MCD spectra using eq 5,[41,47] where σ refers to the Gaussian bandwidth and $\Delta A/A$ is the maximum excitonic MCD intensity at the leading edge divided by the absorbance at the same energy. The negative sign results from the definition of ΔE_{Zeeman} provided above.

$$\Delta E_{Zeeman} = -\frac{2\sigma\Delta A}{A} \quad (5)$$

Application of eq 5 to the CdSe QD data in Figure 5a yields $\Delta E_{Zeeman} = +0.31$ meV and $g_{eff} = +1.1$ at 6 K and 5 T, in good agreement with previous experimental and theoretical results,[45,48] which both gave $g_{eff} \approx +1.4$ for $d = 3$ nm CdSe nanocrystals. Similarly, application of eq 5 to the TM^{2+}:CdSe QD data in Figure 5 yields $\Delta E_{Zeeman} = -9.4$ meV for the 1.0% Mn^{2+}:CdSe QDs and −10.2 meV for the 1.5% Co^{2+}:CdSe QDs, both at 6 K and 5 T. This analysis is summarized in Table 1, which also includes the 6 K effective Landé g factors for the doped CdSe QDs, calculated from the experimental data as $g_{eff} = \Delta E_{Zeeman}/\mu_B H$ in the small-field limit. These values are temperature dependent, scaling with $\langle S_z \rangle$ as $1/T$. ΔE_{Zeeman}(saturation) values are also included in Table 1. The data in Table 1 demonstrate that these doped CdSe QDs show excitonic Zeeman splittings that are much greater than the ones observed in the undoped CdSe QDs, with inverted splittings and saturation magnetization that reflects magnetization of the TM^{2+} impurities. These are the signatures of sp−d exchange in a true DMS.

The magnitudes of the excitonic Zeeman splittings in these doped QDs agree reasonably well with those of the corresponding bulk materials. For comparison, ΔE_{Zeeman}(saturation) was estimated from the bulk values of $N_0(\alpha-\beta)$ (+1.37 eV for Mn^{2+}:CdSe, +2.149 eV for Co^{2+}:CdSe),[1,49] accounting for antiferromagnetic $TM^{2+}-TM^{2+}$ nearest-neighbor interactions,[1] and the results are included in Table 1. The DMS nanocrystal and bulk ΔE_{Zeeman} values are both very large relative to that of the undoped CdSe nanocrystals. The apparent reduction of ΔE_{Zeeman} in the nanocrystals compared to bulk would be consistent with the recent recognition that dopants are generally excluded from the critical nuclei of semiconductor nanocrystals[33,50] and are only incorporated into the nanocrystal lattices during the subsequent growth stages.[11,14,33,37,50] The exclusion of magnetic dopants from the central cores of DMS QDs, where exciton probability densities are greatest, reduces dopant−exciton overlap and consequently diminishes ΔE_{Zeeman}.[37] Some reduction in ΔE_{Zeeman} has also been predicted to result from the wavevector dependence of the sp−d exchange interaction parameters in quantum confined DMSs.[51] Although the model summarized in Figure 4 describes the major experimental observations in Figures 5−6 well, it does neglect the important influences of crystallite shape anisotropy on electron−hole exchange interactions, g values, and zero-field splittings, and is hindered by inhomogeneous broadening of the optical transitions.[43,52] These limitations could be remedied considerably by single-particle measurements. The demonstration here of strong sp−d exchange interactions provides incentive to pursue such measurements on these colloidal TM^{2+}-doped CdSe QDs in order to shed more light on their attractive physical properties.

In summary, MCD spectroscopy has been used to demonstrate strong sp−d exchange interactions in colloidal Mn^{2+}- and Co^{2+}-doped CdSe nanocrystals. TM^{2+}-doped CdSe nanocrystals were synthesized using an inorganic cluster method, and the results of dopant-specific spectroscopic experiments (ligand-field electronic absorption and EPR spectroscopies) were shown to be consistent with successful substitutional doping of the wurtzite nanocrystals. The TM^{2+} saturation magnetization and inverted A-term polarities of the doped CdSe nanocrystal excitonic MCD intensities provide unambiguous evidence of successful nanocrystal doping. MCD spectroscopy was used to evaluate the magnitudes of the excitonic Zeeman splittings, yielding g_{eff}

$\approx$ 50 at 6 K for both 1.0% Mn^{2+}:CdSe and 1.5% Co^{2+}:CdSe QDs, or $\sim$50 times greater than the excitonic Zeeman splittings of undoped CdSe nanocrystals under the same conditions. These results demonstrate that the colloidal TM^{2+}-doped CdSe DMS nanocrystals prepared here are attractive materials for studying spin effects in free-standing quantum-confined semiconductor nanostructures relevant to spin-based information processing.

Acknowledgment. This research was supported by the National Science Foundation (PECASE DMR-0239325), the Research Corporation, the Dreyfus Foundation, and the Sloan Foundation. The authors are grateful to Prof. Høgni Weihe of the University of Copenhagen for graciously providing SIM (version 2002), used for EPR simulations, and to Dr. Chongmin Wang (PNNL) for assistance with TEM measurements. TEM measurements were performed at EMSL, a national user facility sponsored by the U.S. DOE's Office of Biological and Environmental Research located at PNNL and operated by Battelle. NIH Center grant P30 ES07033 is acknowledged for supporting the X-band EPR instrument at UW.

Supporting Information Available: Additional experimental information. This material is available free of charge via the Internet at http://pubs.acs.org.

References

(1) Furdyna, J. K.; Kossut, J., Ed. *Diluted Magnetic Semiconductors*; Semiconductors and Semimetals; Willardson, R. K., Beer, A. C., Eds.; Academic Press: New York, 1988; Vol. 25.
(2) Jungwirth, T.; Sinova, J.; Masek, J.; Kucera, J.; MacDonald, A. H. *Rev. Mod. Phys.* **2006**, *78*, 809−864.
(3) Zutic, I.; Fabian, J.; Das Sarma, S. *Rev. Mod. Phys.* **2004**, *76*, 323−410.
(4) Wolf, S. A.; Awschalom, D. D.; Buhrman, R. A.; Daughton, J. M.; von Molnár, S.; Roukes, M. L.; Chthelkanova, A. Y.; Treger, D. M. *Science* **2001**, *294*, 1488−1495.
(5) Awschalom, D. D.; Flatté, M. E.; Samarth, N. *Sci. Am.* **2002**, *286*, 66−73.
(6) Jonker, B. T.; Park, Y. D.; Bennett, B. R.; Cheong, H. D.; Kioseoglou, G.; Petrou, A. *Phys. Rev. B* **2000**, *62*, 8180−8183.
(7) Rüster, C.; Borzenko, T.; Gould, C.; Schmidt, G.; Molenkamp, L. W.; Liu, X.; Wojtowicz, T. H.; Furdyna, J. K.; Yu, Z. G.; Flatté, M. E. *Phys. Rev. Lett.* **2003**, *91*, 216602.
(8) Ohno, Y.; Young, D. K.; Beschoten, B.; Matsukura, F.; Ohno, H.; Awschalom, D. D. *Nature* **1999**, *402*, 790−792.
(9) Kotov, N. A., Ed. *Nanoparticle Assemblies and Superstructures*; CRC Press LLC: Boca Raton, FL, 2006.
(10) Lu, W.; Lieber, C. M. *J. Phys. D: Appl. Phys.* **2006**, *39*, R387−R406.
(11) For a review see: Bryan, J. D.; Gamelin, D. R. *Prog. Inorg. Chem.* **2005**, *54*, 47−126.
(12) Chen, W., Ed. *J. Nanosci. Nanotechnol.* **2005**, *5*, Special Issue on Doped Nanomaterials and references therein.
(13) Mikulec, F. V.; Kuno, M.; Bennati, M.; Hall, D. A.; Griffin, R. G.; Bawendi, M. G. *J. Am. Chem. Soc.* **2000**, *122*, 2532−2540.
(14) Erwin, S. C.; Zu, L. J.; Haftel, M. I.; Efros, A. L.; Kennedy, T. A.; Norris, D. J. *Nature* **2005**, *436*, 91−94.
(15) Dalpian, G. M.; Chelikowsky, J. R. *Phys. Rev. Lett.* **2006**, *96*, 226802.
(16) Hanif, K. M.; Meulenberg, R. W.; Strouse, G. F. *J. Am. Chem. Soc.* **2002**, *124*, 11495−11502.
(17) Raola, O. E.; Strouse, G. F. *Nano Lett.* **2002**, *2*, 1443−1447.
(18) Chengelis, D. A.; Yingling, A. M.; Badger, P. D.; Shade, C. M.; Petoud, S. *J. Am. Chem. Soc.* **2005**, *127*, 16752−16753.
(19) Meulenberg, R. W.; Van Buuren, T.; Hanif, K. M.; Willey, T. M.; Strouse, G. F.; Terminello, L. J. *Nano Lett.* **2004**, *4*, 2277−2285.
(20) Magana, D.; Perera, S. C.; Harter, A. G.; Dalal, N. S.; Strouse, G. F. *J. Am. Chem. Soc.* **2006**, *128*, 2931−2939.
(21) Jian, W. B.; Fang, J.; Ji, T.; He, J. *Appl. Phys. Lett.* **2003**, *83*, 3377−3379.
(22) Guo, B. C.; Pang, Q.; Yang, C. L.; Ge, W. K.; Yang, S. H.; Wang, J. N. *AIP Conf. Proc.* **2005**, *772*, 605−606.
(23) Norberg, N. S.; Gamelin, D. R. *J. Appl. Phys.* **2005**, *99*, 08M104.
(24) Radovanovic, P. V.; Gamelin, D. R. *J. Am. Chem. Soc.* **2001**, *123*, 12207−12214.
(25) Dabbousi, B. O.; Rodriguez-Viejo, J.; Mikulec, F. V.; Heine, J. R.; Mattoussi, H.; Ober, R.; Jensen, K. F.; Bawendi, M. G. *J. Phys. Chem. B* **1997**, *101*, 9463−9475.
(26) Peng, X.; Schlamp, M. C.; Kadavanich, A. V.; Alivisatos, A. P. *J. Am. Chem. Soc.* **1997**, *119*, 7019−7029.
(27) Dance, I. G.; Choy, A.; Scudder, M. L. *J. Am. Chem. Soc.* **1984**, *106*, 6285−6295.
(28) Eichhöfer, A. *Eur. J. Inorg. Chem.* **2005**, 1245−1253.
(29) Archer, P. I.; Santangelo, S. A.; Gamelin, D. R. **2007**, manuscript in preparation.
(30) Cumberland, S. L.; Hanif, K. M.; Javier, A.; Khitrov, G. A.; Strouse, G. F.; Woessner, S. M.; Yun, C. S. *Chem. Mater.* **2002**, *14*, 1576−1584.
(31) Radovanovic, P. V.; Norberg, N. S.; McNally, K. E.; Gamelin, D. R. *J. Am. Chem. Soc.* **2002**, *124*, 15192−15193.
(32) Archer, P. I.; Radovanovic, P. V.; Heald, S. M.; Gamelin, D. R. *J. Am. Chem. Soc.* **2005**, *127*, 14479−14487.
(33) Schwartz, D. A.; Norberg, N. S.; Nguyen, Q. P.; Parker, J. M.; Gamelin, D. R. *J. Am. Chem. Soc.* **2003**, *125*, 13205−13218.
(34) West, A. R. *Solid State Chemistry*; Wiley: Chichester, U.K., 1992.
(35) Yu, W. W.; Qu, L.; Guo, W.; Peng, X. *Chem. Mater.* **2003**, *15*, 2854−2860.
(36) Langer, J. M.; Baranowski, J. M. *Phys. Status Solidi B* **1971**, *44*, 155−166.
(37) Norberg, N. S.; Parks, G. L.; Salley, G. M.; Gamelin, D. R. *J. Am. Chem. Soc.* **2006**, *128*, 13195−13203.
(38) Title, R. S. *Phys. Rev.* **1963**, *130*, 17−19.
(39) Norberg, N. S.; Kittilstved, K. R.; Amonette, J. E.; Kukkadapu, R. K.; Schwartz, D. A.; Gamelin, D. R. *J. Am. Chem. Soc.* **2004**, *126*, 9387−9398.
(40) Piepho, S. B.; Schatz, P. N. *Group Theory in Spectroscopy with Applications to Magnetic Circular Dichroism*; Wiley: New York, 1983.
(41) Hoffman, D. M.; Meyer, B. K.; Ekimov, A. I.; Merkulov, I. A.; Efros, A. L.; Rosen, M.; Counio, G.; Gacoin, T.; Boilot, J.-P. *Solid State Commun.* **2000**, *114*, 547−550.
(42) Norris, D. J.; Yao, N.; Charnock, F. T.; Kennedy, T. A. *Nano Lett.* **2001**, *1*, 3−7.
(43) Leger, Y.; Besombes, L.; Maingault, L.; Ferrand, D.; Mariette, H. *Phys. Rev. Lett.* **2005**, *95*, 047403.
(44) Ando, K.; Yamada, Y.; Shakin, V. A. *Phys. Rev. B* **1993**, *47*, 13462−13465.
(45) Kuno, M.; Nirmal, M.; Bawendi, M. G.; Efros, A.; Rosen, M. *J. Chem. Phys.* **1998**, *108*, 4242−4247.
(46) Gennser, U.; Liu, X. C.; Vu, T. Q.; Heiman, D.; Fries, T.; Shapira, Y.; Demianiuk, M.; Twardowski, A. *Phys. Rev. B* **1995**, *51*, 9606−9611.
(47) Hofmann, D. M.; Oettinger, K.; Efros, A. L.; Meyer, B. K. *Phys. Rev. B* **1997**, *55*, 9924−9928.
(48) Gupta, J. A.; Awschalom, D. D.; Efros, A. L.; Rodina, A. V. *Phys. Rev. B* **2002**, *66*, 125307.
(49) Kacman, P. *Semicond. Sci. Technol.* **2001**, *16*, R25−R39.
(50) Bryan, J. D.; Schwartz, D. A.; Gamelin, D. R. *J. Nanosci. Nanotechnol.* **2005**, *5*, 1472−1479.
(51) Bhattacharjee, A. K. *Phys. Rev. B* **1998**, *58*, 15660−15665.
(52) Norris, D. J.; Efros, A. L.; Rosen, M.; Bawendi, M. G. *Phys. Rev. B* **1996**, *53*, 16347−16354.

NL0702362